The Astrophysical Journal, 854:58 (7pp), 2018 February 10 https://doi.org/10.3847/1538-4357/aaa6d3

Thermal Emission in the Quiescent Neutron Star SAX J1810.8-2609

Jessamyn L. Allen[1,2], Jeroen Homan[2,3], Deepto Chakrabarty[1,2], and Michael Nowak[2]
[1] Department of Physics, Massachusetts Institute of Technology, 77 Massachusetts Avenue, Cambridge, MA 02139, USA; allenjl@mit.edu
[2] Kavli Institute for Astrophysics and Space Research, MIT, 70 Vassar Street, Cambridge, MA 02139, USA
[3] SRON, Netherlands Institute for Space Research, Sorbonnelaan 2, 3584 CA Utrecht, The Netherlands
Received 2017 September 5; revised 2018 January 5; accepted 2018 January 8; published 2018 February 12

Abstract

We have observed the neutron star low-mass X-ray binary SAX J1810.8−2609 in quiescence with *XMM-Newton*. SAX J1810.8−2609 is one of the faintest non-pulsing neutron star low-mass X-ray binaries in quiescence and previously only had upper limits on its quiescent thermal emission. We found SAX J1810.8−2609 at the same 0.5–10 keV, unabsorbed luminosity as the previous quiescent observation in 2003, $L_X = 1.5 \times 10^{32}$ erg s^{-1}. We show that the spectrum requires both thermal and nonthermal components, each contributing approximately half the total emission. The low neutron star luminosity suggests a time-averaged outburst accretion rate of $\dot{M} \approx 10^{-12}$ $M_\odot$ yr^{-1}, in conflict with its observed outburst activity corresponding to a mass accretion rate that is an order of magnitude larger ($\dot{M} \approx 10^{-11}$ $M_\odot$ yr^{-1}). Our observation designates SAX J1810.8−2609 more firmly as a member of a population of faint quiescent neutron star LMXBs whose quiescent thermal luminosity is not aligned with standard cooling models.

Key words: stars: neutron – X-rays: binaries – X-rays: individual (SAX J1810.8-2609)

1. Introduction

Transient neutron star (NS) low-mass X-ray binaries (LMXBs) exhibit periods of low and high accretion rates onto the NS surface known as quiescence and outburst, characterized by luminosities in the ranges of $10^{31–33}$ erg s^{-1} (0.5–10 keV) and $10^{34–38}$ erg s^{-1}, respectively. The sources spend most of their time in quiescence, with outburst periods typically lasting weeks to months. NS LMXBs can be distinguished by the peak luminosity reached in outburst. Bright transients have peak persistent outburst emission in the range of $L_X = 10^{37–39}$ erg s^{-1}; faint transients peak in the range of $10^{36–37}$ erg s^{-1} and very-faint transients peak $10^{34–36}$ erg s^{-1}. For faint and very faint NS LMXBs, the low outburst luminosity makes it difficult to monitor their outburst activity, especially when the outbursts are short (<week long). Their peak outburst flux can be near or below the sensitivity threshold of most X-ray surveys. Additionally, the outburst durations are often comparable to the monitoring cadences, making these sources easier to miss.

Accretion flows at low rates are not well understood. This regime includes the quiescent state of NS LMXBs, where the accretion rate onto the NS surface is very low. The quiescent X-ray spectrum is typically characterized by two components: one nonthermal and one thermal. The nonthermal component, often modeled with a power law, dominates the spectrum above 2 keV and has been attributed to the low-level accretion flow near the NS (Campana et al. 1998; Menou et al. 1999). Observationally, the nonthermal emission's contribution to the total unabsorbed flux is at a minimum near 10^{33} erg s^{-1} (Jonker et al. 2004a). Above $\approx 10^{33}$ erg s^{-1}, the hard emission's relative flux contribution increases toward larger fractions. Recent observations of the high-energy spectrum (>10 keV) associate it with thermal bremsstrahlung emission (Chakrabarty et al. 2014) possibly produced by the NS boundary layer (D'Angelo et al. 2015). While the nonthermal component's fractional contribution also increases toward lower quiescent luminosities below 10^{33} erg s^{-1}, it is unclear whether the hard quiescent emission is produced by the same physical mechanism in the two luminosity regimes. Below $\approx 10^{32}$ erg s^{-1}, a radio pulsar may turn on producing significant nonthermal synchrotron emission (Stella et al. 1994; Campana et al. 1998).

Despite the nonthermal component's increasing contribution to the quiescent flux at lower luminosities, transiently accreting NSs are expected to exhibit a minimum thermal luminosity set by their time-averaged outburst mass accretion rate. While low-level accretion onto the NS can potentially produce thermal emission in quiescence (Zampieri et al. 1995), even in the complete absence of quiescent accretion the NS is expected to radiate a stable level of thermal emission. The energy source is latent heat generated in the inner crust during accretion. Known as *deep crustal heating*, matter accreted during outbursts compresses the upper layers of the NS, activating density-sensitive pycnonuclear reactions (Brown et al. 1998). The heat is conducted throughout the NS and partially radiated away at the surface, emerging as a thermal spectrum with a predicted surface temperature in the X-ray band.

For a given outburst history (parameterized by a time-averaged accretion rate $\dot{M}$), one can estimate the quiescent NS thermal luminosity L_{NS}. The calculation requires assumptions about the heat released by the pycnonuclear reactions per accreted nucleon (commonly assumed $Q_{nuc} \approx 1.5$ MeV$/m_p$; Brown et al. 1998), as well as standard cooling mechanisms active within the NSs which, in turn, depend on the NS composition. Many NS LMXB transients, including most accretion-powered millisecond pulsars (AMXPs), only have upper limits measured for their thermal luminosities, and even these upper limits fall below the standard cooling predictions (see Figure 8 of Heinke et al. 2010). AMXPs typically exhibit faint ($L_X < 10^{32}$ erg s^{-1}), hard ($\Gamma = 1$–2) spectra in quiescence with little or no NS thermal emission (Campana et al. 2002; Wijnands et al. 2005). These systems are identified as pulsars by pulsations detected in outburst and, in some cases, radio emission in low-luminosity quiescent states. Some NS LMXBs that have not exhibited pulsations in outburst, and, thus, are not likely AMXPs, (e.g., XTE J2123−058, SAX J1810.8−2609, and EXO 1747−214), are also faint in quiescence with low or nonexistent constraints on the thermal surface emission (Jonker et al. 2004b; Tomsick et al. 2004, 2005). These sources also disagree with deep crustal heating predictions.

NS LMXBs whose faint quiescent thermal emission is in conflict with standard heating and cooling models may harbor massive NSs (Colpi et al. 2001), NSs with hybrid crusts (Armas Padilla et al. 2013), or have true outburst histories that are not well represented by the existing observations (Tomsick et al. 2004; Jonker et al. 2007). Enhanced cooling mechanisms (i.e., the direct Urca process) may produce low-temperature NSs below standard cooling model predictions; due to the high density thresholds of the reactions ($\rho > 1.3 \times 10^{15}$ g cm^{-3}), they are only thought to occur in massive NSs, $M_{\rm NS} > 1.7\, M_{\odot}$ (Colpi et al. 2001). Alternatively, deep crustal heating may not be fully active in LMXBs with hybrid NS crusts. In young LMXBs, where the NS has not been accreting for a long time ($\lesssim 10^{8}$ years) and also in systems with very low outburst accretion rates ($\dot{M} \lesssim 10^{-12}\ M_{\odot}$ yr^{-1}), the NS has not accreted enough companion material to activate all the pycnonuclear reactions (Wijnands et al. 2013). Heating is suppressed and the result is a cold NS, $L_{\rm NS} \lesssim 10^{31}$ erg s^{-1}. Deep crustal heating predictions of the quiescent NS thermal luminosity also rely on the time-averaged outburst accretion rate. For most NS LMXBs, there are large uncertainties in the outburst history because the outburst activity over the past 30–40 years is assumed to be the same as the activity over the past several *thousand* years. The outburst history uncertainty is large, particularly for faint or very-faint transients, because their low outburst luminosities can be missed by X-ray monitoring.

SAX J1810.8−2609 is an X-ray transient discovered with the Wide Field Camera on board the *BeppoSAX* satellite (Ubertini et al. 1998). Outbursts have been observed from this source in 1998, 2007, and 2012. During its first observed outburst in 1998, the source exhibited a type-I X-ray burst, identifying SAX J1810.8−2609 as a NS LMXB (Ubertini et al. 1998; Cocchi et al. 1999). The burst showed signs of photospheric radius expansion and a source distance of $d = 4.9 \pm 0.3$ kpc was determined (Natalucci et al. 2000). The persistent outburst emission was approximately 9×10^{35} $(d/4.9\ {\rm kpc})^{2}$ erg s^{-1} (2–10 keV), and the outburst lasted at least 13 days. A later look at the *RXTE* ASM light curve revealed that the source was likely in outburst as early as 1997 December 18, corresponding to an outburst duration of ≈100 days (Tomsick et al. 2004). Additionally, the X-ray luminosity estimated from the 1.5 to 12 keV ASM light curve implied that SAX J1810.8−2609 was significantly brighter earlier in the outburst ($L_{\rm peak} = 1.0 \times 10^{37}$ $(d/4.9\ {\rm kpc})^{2}$ erg s^{-1}, 2–10 keV) compared to when it was observed by *BeppoSAX* in 1998 March.

SAX J1810.8−2609 went into outburst again in 2007. A *Swift* monitoring program for very-faint X-ray transients was triggered on 2007 August 9 (Degenaar et al. 2007). *INTEGRAL* observations occurred between 2007 August 25 and September 30 (Fiocchi et al. 2009). The source was not detected in *Swift*/XRT observations on 2007 November 3 and 5, indicating that SAX J1810.8−2609 was returning to quiescence (Linares et al. 2007) after an outburst duration of 85–92 days. Fiocchi et al. (2009) reported a bolometric outburst luminosity of $L_{\rm X} \approx 5 \times 10^{36}$ $(d/4.9\ {\rm kpc})^{2}$ erg s^{-1} (0.1–500 keV) and classified SAX J1810.8−2609 as a faint X-ray transient, despite Tomsick et al. (2004) reporting a significantly brighter peak outburst luminosity for the 1997/1998 outburst.

In 2012, SAX J1810.8−2609 was seen in outburst with *MAXI* between May 7 and 24 and was found with a $L_{\rm X} \gtrsim 10^{36}$ erg s^{-1} for ∼17 days (Degenaar & Wijnands 2013). It was estimated to have an average 2–20 keV luminosity of $L_{\rm X} = 4.7 \times 10^{36}$ $(d/4.9\ {\rm kpc})^{2}$ erg s^{-1} and a peak value of $L_{\rm X} = 1.5 \times 10^{37}$ $(d/4.9\ {\rm kpc})^{2}$ erg s^{-1}. A *Swift*/XRT observation on 2012 May 12 found SAX J1810.8−2609 with $L_{\rm X} = 2.0 \times 10^{37}$ $(d/4.9\ {\rm kpc})^{2}$ erg s^{-1} (2–10 keV), consistent with the peak luminosity measured with *MAXI* (Degenaar & Wijnands 2013).

SAX J1810.8−2609 has only been observed once previously while in quiescence. In 2003, a 35 ks *Chandra* observation revealed the quiescent spectrum was not consistent with pure thermal emission (Jonker et al. 2004b); blackbody and NS atmosphere models lead to poor reduced chi-squared values ($\chi^2_{\nu} > 1.5$). The spectrum was well-fit with a single power law. While the power law's high photon index ($\Gamma = 3.3 \pm 0.5$) suggested a thermal component was present, adding a soft component was not statistically required. With fewer than 150 source counts and fitting a spectrum binned to fewer than 10 counts per bin, only weak constraints could be placed on an additional soft component. SAX J1810.8−2609's 0.5–10 keV unabsorbed luminosity was estimated to be 1×10^{32} erg s^{-1}, assuming a distance of 4.9 kpc. The thermal component contributed approximately half of the unabsorbed flux, which is treated as an upper limit to the system's NS thermal luminosity. Based on deep crustal heating models and assuming standard cooling processes, the low quiescent thermal luminosity of SAX J1810.8−2609 required an extremely low time-averaged mass accretion rate of $\sim 5.7 \times 10^{-13}\, M_{\odot}$ yr^{-1} (Jonker et al. 2004b). In contrast, estimates of the time-averaged mass accretion rate from the outburst history are considerably larger, $(2 - 5) \times 10^{-12}\ M_{\odot}$ yr^{-1} (Tomsick et al. 2004; Fiocchi et al. 2009), and some are over an order of magnitude higher ($< 1.5 \times 10^{-11}\ M_{\odot}$ yr^{-1}; Heinke et al. 2007).

We obtained a new observation of SAX J1810.8−2609 in quiescence with *XMM-Newton*, which we present here. We find that the quiescent spectrum requires a thermal component that is likely a cooling NS, but that the NS luminosity remains in disagreement with its observed outburst activity and standard cooling models.

2. Observations

2.1. XMM EPIC

SAX J1810.8−2609 was observed on 2015 October 9 (ObsID 0763100101) with the all three instruments (pn, MOS1, MOS2; Strüder et al. 2001; Turner et al. 2001) of the European Photon Imaging Camera (EPIC) on board the *XMM-Newton* focusing X-ray telescope. The 78 ks exposure began at 15:43 UT. All three imaging cameras were used in the small window mode ($63 \times 64/100 \times 100$ pixel area for pn/MOS, respectively) with a timing resolution of 6 ms for pn and 0.3 s for MOS1 and MOS2. The medium optical-blocking filter was used.

We used the *XMM-Newton* Scientific Analysis System (SAS) v16.0.0 with the most recent calibration files (as of 2017 March) to reprocess the data using *epproc*/*emproc* to generate new event files using standard filtering. The beginning of the observation was heavily affected by background flares; for pn/MOS, we excluded times where the 10–12 keV count rate was above 0.05/0.2 cts s^{-1} to provide the best background subtraction. We used the *eregionanalyse* tool to optimize the

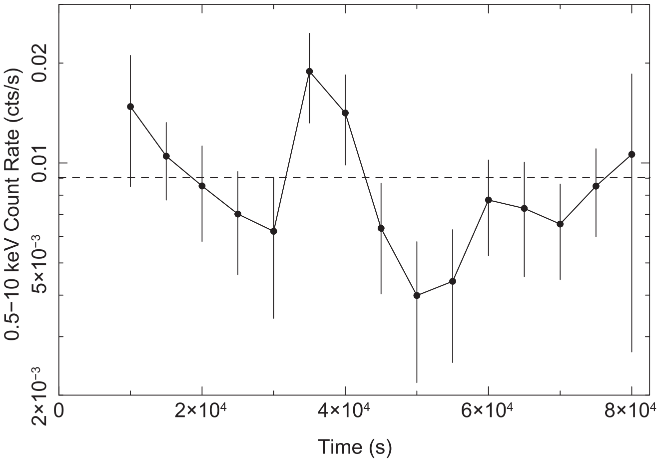

Figure 1. *XMM* pn 0.5–10 keV, background subtracted source light curve with 5 ks bins for SAX J1810.8−2609. The average count rate, indicated by the dashed line, is 9×10^{-3} counts s^{-1}.

source extraction regions, which were determined to be circles with radii of 11″ for both pn and MOS. The background spectrum was extracted from nearby circular regions with radii 35″/20″ for pn/MOS. We used *rmfgen* and *arfgen* to produce the redistribution matrix files and ancillary response files. The net exposures for pn and MOS instruments were 36 and 51 ks (for each MOS camera). The pn light curve is shown in Figure 1.

Using the SAS *edetect_chain* tool, we detected three faint sources within our field of view in addition to SAX J1810.8−2609. Two of these sources were consistent with the coordinates reported by Jonker et al. (2004b) for CXOU J181042.0−261103 and CXOU J181043.5−261044. Their 0.5–10 keV count rates in the pn camera were 0.0037 ± 0.0004 s^{-1} and 0.0027 ± 0.0004 s^{-1}, respectively.

The third faint source was outside the previous *Chandra* observation's field of view and does not correspond to any known X-ray object in the *Simbad* database.[4] It has coordinates R.A. = $18^h10^m37\overset{s}{.}9$, decl. = −26°08′48″ (equinox J2000.0), with an error radius of 2 arcsec. We designate this uncataloged source as XMMU J181037.9−260848. Its 0.5–10 keV count rate in the pn camera was 0.0044 ± 0.0004 s^{-1}. Its spectrum can be fit with an absorbed power-law model ($N_H = 0.6^{+0.7}_{-0.4} \times 10^{22}$ cm^{-2}, $\Gamma = 1.4 \pm 0.5$, $\chi^2_\nu = 0.63$), corresponding to a 0.5–10 keV flux of 4×10^{-14} erg cm^{-2} s^{-1}.

2.2. *Chandra ACIS-S*

We reprocessed the archival *Chandra* observation of SAX J1810.8−2609 (ObsID 3827) from 2003 August 16 in order to compare our *XMM* quiescent findings to those reported by Jonker et al. (2004b). The observation used the S3 CCD of the Advanced CCD Imaging Spectrometer S-array (ACIS-S) in a 1/8 windowed mode. The 35 ks observation was processed with the *chandra_repro* script with CIAO v4.9 (Fruscione et al. 2006) and CALDB 4.5.0. Source and background spectra were extracted from circular regions with radii 4$\overset{''}{.}$9 and 25″, respectively. The net exposure was 32 ks.

[4] http://simbad.u-strasbg.fr/simbad/

3. Analysis and Results

All spectral analysis was performed within ISIS[5] version 1.6.2–30 (Houck et al. 2013). Errors on fit parameters were calculated with *conf_loop* and correspond to the 90% confidence bounds ($\sigma = 1.6$, $\Delta\chi^2 = 2.71$). All quoted chi-squared values, χ^2_ν (dof), are reduced. We used the *cflux* convolution model to calculate the 0.5–10 keV (absorbed) fluxes and (unabsorbed) luminosities. Luminosities are calculated assuming a distance of 4.9 kpc.

We first fit the *XMM* EPIC and *Chandra* ACIS observations separately. For the pn, MOS1, and MOS2 instruments we had 234, 82, and 102 source counts in the 0.5–10 keV range. The *Chandra* observation had 123 source counts. The *XMM* EPIC data were fit simultaneously in the 0.5–10 keV energy range and binned to a minimum of 20 counts per bin, which allows us to use the χ^2_ν statistic to judge the goodness-of-fit.

Fitting the *XMM* data, we applied the *constant* model to correct for offsets between the 3 instruments. We fixed the *constant* factors to 1.0, 1.08, and 1.06, respectively for the pn, MOS1, and MOS2 data based on Table 3 of Tsujimoto et al. (2011).[6] The MOS1 and MOS2 data sets were not combined.

In all of our spectral fits, the NS LMXB continuum was multiplied by the *tbnew* model (v2.3) to account for the neutral ISM absorption; the abundances were set to those of Wilms et al. (2000) and the cross-sections were set to those of Verner et al. (1996). Previous observations of SAX J1810.8−2609, in quiescence and in outburst, constrained the column density along the line of sight to the range of (3–7) $\times 10^{21}$ cm^{-2} (Dickey & Lockman 1990; Natalucci et al. 2000; Degenaar & Wijnands 2013). We allowed the column density to vary in all of our spectral fits.

We fit continuum models typically exhibited by NS LMXBs in quiescence: single component nonthermal (*powerlaw*) and thermal (*bbodyrad* and *NSATMOS*), as well as combinations of nonthermal and thermal components. While a *bbodyrad* model is not a physically accurate model for NS surface emission, it does provide a good fit to thermal emission for faint quiescent spectra with low count numbers. For a blackbody, we allowed the normalization to vary, while for the NS atmosphere model, *NSATMOS*, we fixed the normalization to unity, assuming the entire NS surface produces the thermal emission. *NSATMOS* and *NSA* are both models specifically designed for quiescent surface emission; we found no statistical difference in our fits when using the *NSATMOS* and *NSA* as the NS component, thus we only list results from the *NSATMOS* fits. NS mass and radius are parameters in the NS atmosphere models, as well as the distance to the system. The distance to SAX J1810.8−2609 was fixed to 4.9 kpc (Natalucci et al. 2000). We fixed the mass and radius 1.4 $M_\odot$ and 12 km, adopting the NS values measured from modeling the photospheric radius expansion bursts of SAX J1810.8−2609. Nättilä et al. (2016) and Suleimanov et al. (2017) found $M = 1.3$–1.5 $M_\odot$ and $R = 11.5$–13 km for the NS in SAX J1810.8−2609 using improved cooling tail modeling of hard-state bursts. Results from our continuum fits are listed in Table 1. We also calculated the 0.5–10 keV absorbed fluxes, 0.5–10 kev

[5] http://space.mit.edu/cxc/isis/

[6] We note that Madsen et al. (2017) also performed a cross-calibration of the *XMM-Newton* instruments, as well a cross-calibration of *Chandra* and *XMM-Newton*, but because their analysis only included ACIS-S with the gratings, we were unable to utilize their results in our analysis.

Table 1
Continuum Parameters

Model[a]	$N_{H,22}$	kT[b] (eV)	Norm[c] (km)^2	Γ	Flux[d] (10^{-14} erg s^{-1} cm^{-2})	L_X[e] (10^{32} erg s^{-1})	NS Fraction[f]	χ^2_ν (dof)
				XMM EPIC, Binning = 20 cts bin^{-1}				
Powerlaw	$0.47^{+0.21}_{-0.17}$			$3.2^{+0.3}_{-0.2}$	1.8 ± 0.3	1.1 ± 0.1		1.53 (21)
BBodyrad	<0.04	351^{+50}_{-58}	$0.024^{+0.013}_{-0.008}$		1.4 ± 0.2	0.41 ± 0.05		1.95 (21)
NSATMOS	$0.67^{+0.17}_{-0.11}$	74^{+3}_{-2}	1*		1.2 ± 0.1	1.1 ± 0.3		2.73 (22)
BBodyrad+Powerlaw	$0.29^{+0.38}_{-0.25}$	215^{+106}_{-83}	$0.236^{+15.679}_{-0.204}$	$1.1^{+1.9}_{-1.5}$	3.0 ± 0.6	1.1 ± 0.2	0.41 ± 0.10	1.40 (19)
NSATMOS+Powerlaw	$0.52^{+0.15}_{-0.11}$	67^{+5}_{-6}	1*	$1.5^{+1.0}_{-0.9}$	3.2 ± 0.6	1.5 ± 0.2	0.58 ± 0.19	1.32 (20)
				Joint *XMM* EPIC and *Chandra* ACIS, Binning = 20 cts bin^{-1}				
Powerlaw	$0.46^{+0.18}_{-0.14}$			$3.3^{+0.2}_{-0.2}$	1.7 ± 0.2	1.1 ± 0.1		1.36 (26)
BBodyrad	<0.05	341^{+51}_{-38}	$0.027^{+0.010}_{-0.010}$		1.4 ± 0.2	0.42 ± 0.05		1.85 (26)
NSATMOS	$0.72^{+0.12}_{-0.14}$	74^{+2}_{-3}	1*		1.1 ± 0.1	1.2 ± 0.2		2.73 (27)
BBodyrad+Powerlaw	$0.30^{+0.36}_{-0.23}$	206^{+57}_{-93}	$0.292^{+20.971}_{-0.247}$	$1.3^{+0.7}_{-1.1}$	2.7 ± 0.7	1.1 ± 0.3	0.41 ± 0.17	1.22 (24)
NSATMOS+ Powerlaw	$0.53^{+0.12}_{-0.12}$	68^{+3}_{-9}	1*	$1.3^{+1.3}_{-0.8}$	2.8 ± 0.4	1.5 ± 0.2	0.58 ± 0.18	1.15 (25)

Notes.
[a] For all models: $M = 1.4\ M_\odot$, $R = 12$ km, $D = 4.9$ kpc. All continuum models are multiplied by the *constant* model. With 1σ errors, the cross-normalization constants are $C_{pn} = 1.0$, $C_{MOS1} = 1.078 \pm 0.007$, $C_{MOS2} = 1.059 \pm 0.007$, and $C_{ACIS-S3} = 1.194 \pm 0.006$.
[b] Thermal component temperature.
[c] Thermal component normalization. For a blackbody, the normalization has been corrected for the source distance. For *NSATMOS*, the normalization is fixed to 1.
[d] 0.5–10 keV, absorbed *XMM* pn flux.
[e] 0.5–10 keV, unabsorbed *XMM* pn luminosity.
[f] Thermal fraction of the 0.5–10 keV unabsorbed *XMM* pn luminosity.

unabsorbed luminosities and the thermal fractional contribution for the two-component models.

Our fits to the *XMM* spectrum revealed that a pure power law is a poor fit, $\chi^2_\nu = 1.5$; the power law cannot produce the high-energy emission (>4 keV) seen in the pn data. The high power-law index ($\Gamma = 3.2$) indicates that the spectrum is very soft. Pure thermal continuum models, either a blackbody or NS atmosphere, provided even worse fits to the EPIC data, $\chi^2_\nu = 2.0$ and 2.7, respectively. The thermal continuum models do not produce essentially any significant emission above 3 keV, so yet again the high-energy portion of the spectrum was underfit.

Continuum models with both thermal and nonthermal components provided significantly better fits to our *XMM* data, accurately modeling the high-energy portion of the spectrum. The thermal component has temperatures of 215 eV for the blackbody and 67 eV for the NS atmosphere model. The power-law index was significantly harder compared to a pure power-law fit with $\Gamma = 1.1$ and 1.5 when the thermal component is fit with a blackbody and a NS atmosphere model, respectively. The absorbed flux is similar for both two-component continuum prescriptions ($F \approx 3.0 \times 10^{-14}$ erg s^{-1} cm^{-2}, 0.5–10 keV), but the NS atmosphere plus power-law model yields a higher unabsorbed luminosity ($L_X = 1.5 \times 10^{32}$ erg s^{-1}) than the blackbody plus power-law model ($L_X = 1.1 \times 10^{32}$ erg s^{-1}). The thermal and nonthermal components each contribute approximately half to the unabsorbed flux.

The NS atmosphere plus power-law model provides a slightly better fit than the blackbody plus power-law model, but in both cases, the χ^2_ν was significantly lower than the fits with a single component continuum. The F-statistic probability for the NS atmosphere plus power-law fit versus the pure power-law fit is 0.05, indicating that the addition of the NS atmosphere component significantly improved the continuum fit.

The *Chandra* observation was fit in the 0.5–10 keV energy range. Binning to 20 counts per bin yielded only five bins, so for models with more than four fit parameters, the χ^2_ν values were too low (<0.2) to interpret the quality of the fit. Following Jonker et al. (2004b), we binned the spectrum to a minimum of 10 counts per bin and found the same trends in the continuum model fits. A pure power-law continuum yielded a very high ($\Gamma = 3.2$) photon index, while purely thermal models provided poor fits to the *Chandra* data. Adding a power-law component improved the fits compared to single component thermal models, but did not provide a statistical advantage over a pure power-law continuum. The unabsorbed flux of our *XMM* observation is consistent with the *Chandra* value, indicating that the source is found at the same quiescent level in 2015, within errors, as it was in 2003 ($F \approx 3.8 \times 10^{-14}$ erg s^{-1} cm^{-2}, 0.5–10 keV; Jonker et al. 2004b).

Due to the similarity in continuum parameters and the source flux between the *XMM* and *Chandra* observations, we fit the two observations simultaneously. We used the *constant* model to account for offsets between the four instruments, fixing the constants for the *XMM* pn, MOS1, MOS2, and *Chandra* ACIS-S data to 1.0, 1.08, 1.06, and 1.19, respectively, calculated from Table 3 of Tsujimoto et al. (2011). The cross-calibration between *Chandra* and *XMM* EPIC was performed with reference to the S3 chip of ACIS-S, the same CCD used in the 2004 quiescent observation. When we allowed for continuum parameters to vary between the two observations (such as power-law normalization, thermal component temperature, etc.,), we found that the parameters were consistent within their 90% error bounds, so we tied all parameters between the *XMM* and *Chandra* data sets. In the joint fits, we binned both *XMM* and *Chandra* data sets to a minimum of 20 counts per bin to ensure the χ^2_ν was a probe of the goodness of fit.

Jointly fitting the two observations strengthened the results found when fitting the *XMM* spectra by themselves. The

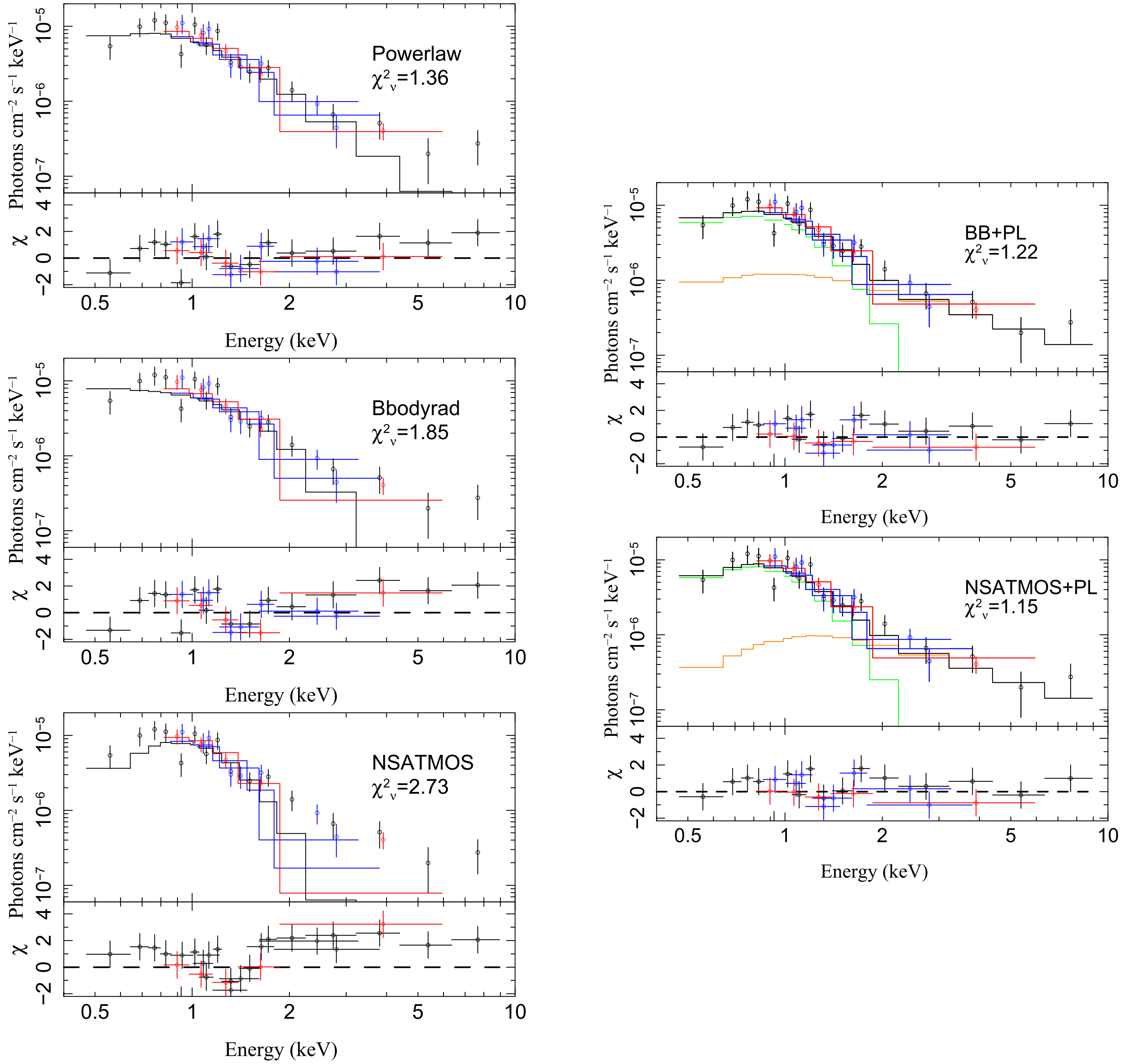

Figure 2. Joint continuum fits to the *XMM* EPIC pn (black), MOS 1/2 (blue), and *Chandra* ACIS-S data (red) for SAX J1810.8−2609, each binned to a minimum of 20 counts per bin. The continuum was tied between all data sets and we fit with nonthermal (top, left), thermal (bottom 2, left), and two-component (right) models. For the two-component continuum, we plot the thermal contribution in green and the nonthermal emission in orange. While the large power-law index for a pure power law suggests that the spectrum is soft and has significant thermal emission, we found the pure thermal models (i.e., *bbodyrad* and *NSATMOS*) were not sufficient; high-energy residuals above 3 keV show that an additional power-law component is required. The *NSATMOS+powerlaw* fit provides the best fit overall.

continuum fits are plotted in Figure 2. A pure power-law model provides a poor fit to the data and a high power-law index, $\Gamma = 3.3 \pm 0.6$. Despite the large photon index, indicating that the spectrum is soft, pure thermal models, either *bbodyrad* or *NSATMOS*, were incomplete descriptions of the data; significant residuals above 3 keV require another component to provide an accurate fit. A two-component model with thermal and nonthermal components provided the best fit to the two data sets. We achieved χ^2_ν values of approximately 1.2 for *bbodyrad+powerlaw* and *NSATMOS+powerlaw* continuum models. The thermal component had temperatures of 205 and 70 eV for blackbody and NS atmosphere models, and the nonthermal component had a relatively hard photon index, $\Gamma \approx 1.3 \pm 1.0$, for both of the two thermal models. The 0.5–10 keV absorbed fluxes and unabsorbed luminosities were the same as those found when the *XMM* data was fit alone, $F \approx 3.0 \times 10^{14}$ erg s^{-1} cm^{-2}, $L_X \approx 1.5 \times 10^{32}$ erg s^{-1}. The thermal and nonthermal components contribute roughly equally to the unabsorbed flux.

4. Discussion

SAX J1810.8−2609 is a NS LMXB for which the previously reported thermal NS luminosity upper limit was in disagreement with NS heating and cooling models (Jonker et al. 2004b). In our new (2015) *XMM* observation, we find the source at the same quiescent level as the 2003 *Chandra* observation, $L_X = 1.5 \times 10^{32}$ erg s^{-1}. A two-component spectrum with a thermal component providing ≈50% of the flux provides the best description of the quiescent spectrum. We interpret the thermal component as a cooling NS surface.

Despite our observation being heavily affected by background flares that reduced our exposure by nearly half, we obtained twice as many source counts compared to the previous, and only, quiescent observation performed over 10 years ago. Most significantly, we measured nearly 30 counts above 4 keV (compared to only 4 counts in the *Chandra* observation), which was necessary to constrain the high-energy portion of the spectrum and distinguish between a completely nonthermal spectrum and a spectrum that required both thermal and nonthermal emission. While a power law provides an equally good fit as a combination model for the 2003 *Chandra* observation, our 2015 *XMM* data required both thermal (either a blackbody or a NS atmosphere) and power-law components to fit the 0.5–10 keV quiescent spectrum. The NS atmosphere model had a temperature of ≈70 eV, which is consistent with the previously reported quiescent thermal temperature (Jonker et al. 2004b) and is also in the range of previously observed quiescent NS temperatures (Brown et al. 1998; Heinke et al. 2003, 2006).

With a NS luminosity of $\approx 10^{32}$ erg s^{-1}, SAX J1810.8−2609 is one of the faintest NSs in a non-AMXP system. Based on deep crustal heating and standard cooling predictions, the NS luminosity in SAX J1810.8−2609 is at least an order of magnitude fainter than expected given its outburst accretion rate history (see Figure 8 in Heinke et al. 2010). Possible explanations for a cold NS include enhanced cooling processes, a hybrid crust, or overestimation of the time-averaged outburst accretion rate.

The density threshold for the direct Urca process is reached inside massive NSs ($M = 1.6$–$1.8\ M_\odot$; Beznogov & Yakovlev 2015). This enhanced cooling mechanism allows for the heat produced by the pycnonuclear reactions to be radiated away more efficiently and significantly reduces the NS cooling timescale ($\tau \ll 10^4$ years; Colpi et al. 2001). In our fits, we fixed the mass and radius values of the NS atmosphere models based on results from burst cooling tail methods. Nättilä et al. (2016) found $M = 1.4 \pm 0.4\ M_\odot$, $R = 12 \pm 0.5$ km (errors are the 68% confidence level), so a heavy NS in SAX J1810.8 −2609 is not excluded at the 1-σ level. Unfortunately, our quiescent data is not able to distinguish between different NS mass and radius values. We were unable to constrain the NS mass even when we fixed the radius parameter. Similarly, the uncertainty in the NS mass in XTE J2123−058 cannot exclude a massive NS, which may explain its low thermal quiescent luminosity ($L_X < 1.4 \times 10^{32}$ erg s^{-1}, bolometric; Tomsick et al. 2004). NS mass measurements using a variety of techniques, including radial velocity curves, find $M_{NS} = 1.5 \pm 0.3\ M_\odot$ (Tomsick et al. 2001, 2002; Casares et al. 2002) and 1.04–1.56 $M_\odot$ (Shahbaz et al. 2003).

A hybrid NS crust, where the original crust has not been completely replaced by compressed accreted material, may be able to produce a cool quiescent NS. If less than 0.02 $M_\odot$ has been accreted, the crust is largely composed of the original NS material and the full range of pycnonuclear reactions will not be activated, resulting in heating less than ≈1.5 MeV per accreted nucleon assumed with deep crustal heating (Wijnands et al. 2013). Young systems and those with extremely low outburst accretion rates are the most likely candidates for hybrid crusts; neither type of system should have accreted enough material to replace the crust during the course of its lifetime. While SAX J1810.8−2609 has a low-mass outburst accretion rate compared to other NS LMXBs ($\dot{M} \lesssim 10^{-11}\ M_\odot$ yr^{-1}), the uncertainties in the source's outburst history, in particular, the variation in the mass accretion rate over the binary's evolutionary timescale, and a general lack of understanding of the heating and cooling mechanisms in a hybrid NS crust prevents us from evaluating a hybrid crust as a possible explanation for the faint NS in SAX J1810.8−2609.

Originally thought to be relatively faint in outburst ($L_{ave} \approx 5 \times 10^{36}$ erg s^{-1}; Natalucci et al. 2000), subsequent reviews of SAX J1810.8−2609's *RXTE* ASM light curves found the source to exhibit brighter peak luminosities ($L_{peak} = 2 \times 10^{37}$ erg s^{-1}) and longer outbursts, $t_{dur} \approx 100$ day (Tomsick et al. 2004). For X-ray transients, the time-averaged outburst mass accretion rate over the past 33 years (Equation (1) from Tomsick et al. 2004) is given by

$$\dot{M} = \frac{\bar{L}_{peak} N t_{otb} f}{\epsilon c^2 (33\ \text{year})}, \quad (1)$$

where $\bar{L}_{peak}$ is the mean peak outburst luminosity, N is the number of outbursts in the past 33 years, t_{otb} is the typical outburst duration, f parameterizes the shape of the outburst light curve, and ϵ is the fraction of the accreted rest mass energy that is released during accretion. For NSs, ϵ is typically 0.2 (Rutledge et al. 2002) and f can be approximated as the mean outburst flux divided by the peak outburst flux.

SAX J1810.8−2609 has had three outbursts in the past 21 years since the commencement of monitoring with *RXTE* and *MAXI* (Natalucci et al. 2000; Fiocchi et al. 2009; Degenaar & Wijnands 2013). Based on the 1997/1998 outburst *RXTE* ASM count rates in Figure 3(c) of Tomsick et al. (2004), we estimate a 0.5–100 keV $F_{peak} = 8 \times 10^{-9}$ erg cm^{-2} s^{-1} and $F_{ave} = 2.7 \times 10^{-9}$ erg cm^{-2} s^{-1} calculated with *WebPimms*[7] assuming a power-law spectrum with $\Gamma = 1.96$ and $N_{H,22} = 0.3$ (Natalucci et al. 2000). The 1997/1998 outburst had a duration of ≈100 day (Tomsick et al. 2004). For the 2007 outburst, which lasted ≈85–92 days (Degenaar & Wijnands 2013), Fiocchi et al. (2009) reported $F_{ave} = 1.6 \times 10^{-9}$ erg cm^{-2} s^{-1} (0.1–500 keV). Estimating the peak flux from the 2–12 keV *RXTE* ASM light curve (Figure 1a), again using a power-law spectrum with $\Gamma = 1.96$ and $N_{H,22} = 0.3$, we found $F_{peak} = 4.9 \times 10^{-9}$ erg cm^{-2} s^{-1} for the 2007 outburst. The 2012 outburst reported by Degenaar & Wijnands (2013) was also bright $L_{peak} = 1.5 \times 10^{37}$ erg s^{-1} (2–10 keV) and $L_{ave} = 4.7 \times 10^{36}$ erg s^{-1}, it may have only lasted ≈20 days. Adapting Equation (1) for the three outbursts exhibited by SAX J1810.8−2609 over the past 21 years, we calculate $\dot{M} = 9 \times 10^{-12}\ M_\odot$ yr^{-1}.

For a quiescent NS heated by pycnonuclear reactions in the crust (i.e., deep crustal heating), the luminosity associated with the cooling NS, L_{NS} is given by (Equation (1) from Rutledge et al. 2002)

$$L_{NS} = 9 \times 10^{32} \left(\frac{\dot{M}}{10^{-11}\ M_\odot\ \text{yr}^{-1}} \right), \quad (2)$$

based on 1.45 MeV of heat deposited in the crust per accreted nucleon (Haensel & Zdunik 1990). For a quiescent luminosity of

[7] https://heasarc.gsfc.nasa.gov/cgi-bin/Tools/w3pimms/w3pimms.pl

$L_X = 1.1 \times 10^{32}$ erg s^{-1} and a 50% thermal contribution, Jonker et al. (2004b) inferred an outburst mass accretion rate of 6×10^{-13} $M_\odot$ yr^{-1}, which was significantly lower than the accretion rate estimated from outburst activity, although at the time only a single outburst had been observed from SAX J1810.8−2609. Our *XMM* observation, which has over twice as many counts as the *Chandra* observation, places the source at a more highly constrained quiescent luminosity, $L_X = 1.5 \times 10^{32}$ erg s^{-1} with a 50% thermal contribution, requiring an outburst accretion rate of $\approx 8 \times 10^{-13}$ $M_\odot$ yr^{-1}.

This value is an order of magnitude lower than the time-averaged mass accretion rate calculated from its observed outburst activity. Referencing Figure 8 in Heinke et al. (2010), again, we find the new, more constraining estimates for the cooling NS luminosity and the time-averaged outburst accretion rate are still in disagreement with standard cooling models.

Even though enhanced cooling via the direct Urca process has not been ruled out by NS mass estimates for the NS in SAX J1810.8−2609, other "fast" neutrino emission processes may be active inside less massive NSs, resulting in enhanced cooling curves (Yakovlev & Pethick 2004; Page et al. 2006; Heinke et al. 2010; Wijnands et al. 2013). The lower NS thermal luminosities (compared to standard "slow" cooling mechanisms) could be produced by pion or kaon processes. These enhanced neutrino cooling pathways have lower density requirements than the direct Urca process and require less massive NSs.

While our new measurement of the NS quiescent luminosity is already inconsistent with deep crustal heating and standard cooling models, there is also the possibility that the thermal component is not actually emission from the NS surface. Low-level accretion flows can produce a thermal-like spectrum (Zampieri et al. 1995), while others have suggested that the nonthermal and thermal quiescent emission may both be associated with the NS boundary layer (Deufel et al. 2002; D'Angelo et al. 2015). Both scenarios imply the cooling NS may not been detected in SAX J1810.8−2609 in quiescence, pushing the source further into disagreement between standard heating and cooling models and the known outburst history. However, the similarity of the quiescent luminosities between the two quiescent observations does not support the interpretation that accretion produces the observed thermal emission in SAX J1810.8−2609. Two outbursts have occurred between the quiescent observations, which were taken over 10 years apart. In both quiescent observations, the source was found with $L_X \approx 1.5 \times 10^{32}$ erg s^{-1}. The consistency between the two observations supports our interpretation that we have observed the cooling NS surface.

This work is based on observations with *XMM-Newton*, an ESA science mission with instruments and contributions directly funded by ESA member states and the USA (NASA). J.L.A. acknowledges support from the *XMM-Newton* Guest Observer program through NASA grant NNX16AE12G. We thank the anonymous referee for constructive criticism.

ORCID iDs

Jessamyn L. Allen https://orcid.org/0000-0001-6758-8345
Jeroen Homan https://orcid.org/0000-0001-8371-2713
Deepto Chakrabarty https://orcid.org/0000-0001-8804-8946
Michael Nowak https://orcid.org/0000-0001-6923-1315

References

Armas Padilla, M., Degenaar, N., & Wijnands, R. 2013, MNRAS, 434, 1586
Beznogov, M. V., & Yakovlev, D. G. 2015, MNRAS, 452, 540
Brown, E. F., Bildsten, L., & Rutledge, R. E. 1998, ApJL, 504, L95
Campana, S., Colpi, M., Mereghetti, S., Stella, L., & Tavani, M. 1998, A&ARv, 8, 279
Campana, S., Stella, L., Gastaldello, F., et al. 2002, ApJL, 575, L15
Campana, S., Stella, L., Mereghetti, S., et al. 1998, ApJL, 499, L65
Casares, J., Dubus, G., Shahbaz, T., Zurita, C., & Charles, P. A. 2002, MNRAS, 329, 29
Chakrabarty, D., Tomsick, J. A., Grefenstette, B. W., et al. 2014, ApJ, 797, 92
Cocchi, M., Bazzano, A., Natalucci, L., et al. 1999, ApL&C, 38, 133
Colpi, M., Geppert, U., Page, D., & Possenti, A. 2001, ApJL, 548, L175
D'Angelo, C. R., Fridriksson, J. K., Messenger, C., & Patruno, A. 2015, MNRAS, 449, 2803
Degenaar, N., Klein-Wolt, M., & Wijnands, R. 2007, ATel, 1175
Degenaar, N., & Wijnands, R. 2013, in IAU Symp. 291, Neutron Stars and Pulsars: Challenges and Opportunities after 80 Years, ed. J. van Leeuwen (Cambridge: Cambridge Univ. Press), 141
Deufel, B., Dullemond, C. P., & Spruit, H. C. 2002, A&A, 387, 907
Dickey, J. M., & Lockman, F. J. 1990, ARA&A, 28, 215
Fiocchi, M., Natalucci, L., Chenevez, J., et al. 2009, ApJ, 693, 333
Fruscione, A., McDowell, J. C., Allen, G. E., et al. 2006, Proc. SPIE, 6270, 62701V
Haensel, P., & Zdunik, J. L. 1990, A&A, 227, 431
Heinke, C. O., Altamirano, D., Cohn, H. N., et al. 2010, ApJ, 714, 894
Heinke, C. O., Grindlay, J. E., Lugger, P. M., et al. 2003, ApJ, 598, 501
Heinke, C. O., Jonker, P. G., Wijnands, R., & Taam, R. E. 2007, ApJ, 660, 1424
Heinke, C. O., Rybicki, G. B., Narayan, R., & Grindlay, J. E. 2006, ApJ, 644, 1090
Houck, J. C., Davis, J., Huenemoerder, D., et al. 2013, ISIS: Interactive Spectral Interpretation System for High Resolution X-Ray Spectroscopy, Astrophysics Source Code Library, ascl:1302.002
Jonker, P. G., Galloway, D. K., McClintock, J. E., et al. 2004a, MNRAS, 354, 666
Jonker, P. G., Steeghs, D., Chakrabarty, D., & Juett, A. M. 2007, ApJL, 665, L147
Jonker, P. G., Wijnands, R., & van der Klis, M. 2004b, MNRAS, 349, 94
Linares, M., Degenaar, N., & Wijnands, R. 2007, ATel, 1260
Madsen, K. K., Beardmore, A. P., Forster, K., et al. 2017, AJ, 153, 2
Menou, K., Esin, A. A., Narayan, R., et al. 1999, ApJ, 520, 276
Natalucci, L., Bazzano, A., Cocchi, M., et al. 2000, ApJ, 536, 891
Nättilä, J., Steiner, A. W., Kajava, J. J. E., Suleimanov, V. F., & Poutanen, J. 2016, A&A, 591, A25
Page, D., Geppert, U., & Weber, F. 2006, NuPhA, 777, 497
Rutledge, R. E., Bildsten, L., Brown, E. F., et al. 2002, ApJ, 580, 413
Shahbaz, T., Zurita, C., Casares, J., et al. 2003, ApJ, 585, 443
Stella, L., Campana, S., Colpi, M., Mereghetti, S., & Tavani, M. 1994, ApJL, 423, L47
Strüder, L., Briel, U., Dennerl, K., et al. 2001, A&A, 365, L18
Suleimanov, V. F., Poutanen, J., Nättilä, J., et al. 2017, MNRAS, 466, 906
Tomsick, J. A., Gelino, D. M., Halpern, J. P., & Kaaret, P. 2004, ApJ, 610, 933
Tomsick, J. A., Gelino, D. M., & Kaaret, P. 2005, ApJ, 635, 1233
Tomsick, J. A., Heindl, W. A., Chakrabarty, D., Halpern, J. P., & Kaaret, P. 2001, ApJL, 559, L123
Tomsick, J. A., Heindl, W. A., Chakrabarty, D., & Kaaret, P. 2002, ApJ, 581, 570
Tsujimoto, M., Guainazzi, M., Plucinsky, P. P., et al. 2011, A&A, 525, A25
Turner, M. J. L., Abbey, A., Arnaud, M., et al. 2001, A&A, 365, L27
Ubertini, P., in 't Zand, J., Tesseri, A., Ricci, D, & Piro, L 1998, IAUC, 6838
Verner, D. A., Ferland, G. J., Korista, K. T., & Yakovlev, D. G. 1996, ApJ, 465, 487
Wijnands, R., Degenaar, N., & Page, D. 2013, MNRAS, 432, 2366
Wijnands, R., Homan, J., Heinke, C. O., Miller, J. M., & Lewin, W. H. G. 2005, ApJ, 619, 492
Wilms, J., Allen, A., & McCray, R. 2000, ApJ, 542, 914
Yakovlev, D. G., & Pethick, C. J. 2004, ARA&A, 42, 169
Zampieri, L., Turolla, R., Zane, S., & Treves, A. 1995, ApJ, 439, 849